



Polymerization pattern characterization within a resin-based composite cured using different curing units at two distances

Afnan O. Al-Zain¹ · George J. Eckert² · Henry Lukic³ · Spiro Megremis³ · Jeffrey A. Platt⁴

Received: 22 January 2018 / Accepted: 25 January 2019 / Published online: 9 February 2019
© Springer-Verlag GmbH Germany, part of Springer Nature 2019

Abstract

Objectives To investigate the relationship of the irradiance-beam-profile areas from six different light-curing units (LCUs) with the degree of conversion (DC), microhardness (KH), and cross-link density (CLD) throughout a resin-based composite (RBC) cured at two clinically relevant distances, and to explore the correlations among them.

Materials and methods A mapping approach was used to measure DC using micro-Raman spectroscopy, KH using a Knoop indenter on a hardness tester, and %KH reduction after ethanol exposure, as an indicator for CLD within a nano-hybrid RBC increment ($n = 3$) at various depths. These sample composites were cured from two distances while maintaining the radiant exposure, using six different light-curing units: one quartz-tungsten-halogen; two single and three multiple-emission-peak light-emitting-diode units. Irradiance beam profiles were generated for each LCU at both distances, and localized irradiance values were calculated. Points across each depth were analyzed using repeated measures ANOVA. Correlations across multiple specimen locations and associations between beam uniformity corresponding with polymerization measurements were calculated using linear mixed models and Pearson correlation coefficients.

Results Significant non-uniform polymerization patterns occurred within the specimens at various locations and depths. At 2-mm curing distance, the localized DC = 52.7–76.8%, KH = 39.0–66.7 kg/mm², and %KH reduction = 26.7–57.9%. At 8-mm curing distance, the localized DC = 50.4–78.6%, KH = 40.3–73.7 kg/mm², and %KH reduction = 28.2–56.8%. The localized irradiance values were weakly correlated with the corresponding DC, KH, and %KH reduction, with only a few significant correlations ($p < 0.05$).

Conclusions Although significant differences were observed at each depth within the specimens, the localized irradiance values for all LCUs did not reflect the polymerization pattern and did not seem to have a major influence on polymerization patterns within the RBC, regardless of the curing distance.

Clinical relevance Commonly used LCUs do not produce uniform polymerization regardless of the curing distance, which may contribute to the risk of RBC fracture.

Keywords Degree of conversion · Microhardness · Cross-link density · Resin composite · Beam profile · Light-curing unit

Electronic supplementary material The online version of this article (<https://doi.org/10.1007/s00784-019-02831-1>) contains supplementary material, which is available to authorized users.

✉ Afnan O. Al-Zain
alzain@kau.edu.sa

¹ Restorative Dentistry Department, Faculty of Dentistry, King Abdulaziz University, P.O. Box: 80209, Jeddah 21589, Saudi Arabia

² Department of Biostatistics, Indiana University School of Medicine, Indiana University Purdue University Indianapolis, Indianapolis, IN, USA

³ Research and Standards, American Dental Association Science Institute, Chicago, IL, USA

⁴ Department of Biomedical and Applied Sciences, Indiana University School of Dentistry, Indiana University Purdue University Indianapolis, Indianapolis, IN, USA

Introduction

Fracture of resin-based composite (RBC) restorations is a common cause for their clinical failure [1, 2]. The incidence of fracture has increased recently from approximately 29 to 39% [2]. There are several contributing factors to RBC fracture including material composition, operator technique, quality of polymerization, and stresses generated during cyclic loading [1, 3, 4]. Characterizing polymerization within the bulk of a restoration may provide a better understanding of the relationship between polymerization and fracture.

Polymerization of light-activated RBC results in a highly cross-linked polymer structure [5, 6]. However, monomer conversion is never complete, and the polymer network contains a considerable amount of unreacted double bonds and

pendant groups [6, 7]. A strong correlation has been suggested between RBC degree of conversion (DC) and hardness [8]. Also, several mechanical and physical properties are associated with DC, hardness, and cross-link density (CLD) [6, 7, 9, 10]. Evaluating both the DC and the CLD of the RBC is important because CLD considers the heterogeneity of the polymer network, unlike DC [11]. Many studies evaluated polymerization effectiveness by obtaining DC and hardness measurements on the top and bottom specimen surfaces, or by sectioning the specimens longitudinally and obtaining hardness measurements along the exposed surfaces [10–14]. Studies that estimated CLD indirectly after ethanol-softening used a limited number of hardness measurements on the top and bottom surfaces [15–17].

Typically, the irradiance beam profile measured from a LCU is not uniform [18–20]. This may be more of a concern for the light-emitting-diode (LED) units compared to the quartz-tungsten-halogen (QTH) units [18–20] because the LED chips are typically side-by-side making complete irradiance uniformity across their light-emitting tips a challenge. However, QTH units exhibit relatively uniform irradiance distributions across their light-emitting tips, and the radiated light is comprised of a broad spectral emission range (380–520 nm), which includes the wavelengths needed by most RBC photoinitiators [19–22]. Single emission peak LED (SLED) units typically contain blue LED chips, with spectral emission curves that range from 400 to 520 nm, which includes the peak absorption range for the common photoinitiator camphorquinone (CQ) [19, 20, 22, 23]. Multiple emission peak LED (MLED) units include an additional violet LED chip, or chips, with a spectral emission between 380 and 420 nm that is in the peak absorption range of some alternative photoinitiators, such as diphenyl (2,4,6-trimethylbenzoyl) phosphine oxide (TPO) [19, 20, 22, 23]. The non-uniform irradiance distribution from the light-emitting tip of a dental curing unit could result in localized discrepancies in photoinitiator activation, free radical production, and reaction rates [24–27]. Ultimately, the overall properties and longevity of a restoration could be impacted [3, 18, 19, 21, 25, 26]. However, not every non-uniform LCU results in unsatisfactory performance of a restoration if the required irradiance (mW/cm^2) is received by the RBC [18, 25, 26, 28]. Increasing the distance between the light-emitting tip and the restoration leads to the restoration receiving less irradiance from the curing unit [3, 19–21, 29]. As a result, increasing the curing time to compensate for the reduction in irradiance received by the restoration with increasing distance may be needed to achieve satisfactory polymerization. Since a clinical setting does not allow for a 0-mm curing distance, it is more clinically relevant to evaluate the performance of a RBC at a distance [29]. Studies reported that 2 and 8-mm curing distances are the best and worst clinical case scenarios,

respectively, which is why these distances were chosen for the present study [27, 29]. In addition, the generated irradiance beam profile from the LCU is reported as more uniform at a further distance compared to at a closer distance [3, 19–21, 29].

The irradiance beam profiles measured from LCUs correspond with the hardness of the RBCs as shown by the hardness mapping on the top and bottom surfaces from one distance [25–27]. However, there is limited understanding of this influence within the bulk of a restoration. Recent work showed that a RBC cured with either a QTH or a MLED unit at one distance, while maintaining a constant radiant exposure, resulted in DC and CLD values that were not uniform throughout the RBC [30]. Therefore, an assessment of the RBC increments cured at two clinically relevant distances was worth further investigation. In addition, exploring correlations between the localized irradiance beam profiles at multiple distances with DC, hardness, and CLD values within a RBC could provide a better understanding of polymerization patterns within a restoration with respect to curing distance.

The aim of this study was to explore the influence of limited regions of irradiance beam profiles from different curing units on the corresponding DC, Knoop microhardness (KH), and CLD values within the RBC at two clinically relevant curing distances, and to explore the correlations among these factors. The working hypotheses were as follows: Limited irradiance beam profile areas from different MLED and SLED units compared to one QTH will result in (1) different DC, KH, and CLD patterns within an RBC increment at two clinically relevant curing distances; (2) significantly greater differences in DC, KH, and CLD values within a RBC increment when cured at a 2-mm curing distance compared to an 8-mm; (3) a strong localized DC correlation with the corresponding KH and CLD values within a RBC increment when cured at two clinically relevant distances; and (4) a strong correlation with the corresponding DC, KH, and CLD values on the top RBC surfaces cured at two clinically relevant distances.

Materials and methods

Six LCUs were explored: one QTH [Optilux 401 (O), Kerr, Orange, CA] served as the control. In addition, three MLED units [Bluephase Style (BS), Ivoclar Vivadent, Amherst, NY] with the updated light guide tip, [SmartLite Max (SM), Dentsply, York, PA], and [Valo Cordless (V), Ultradent, South Gordon, UT]; and two SLED [Demi (D) and Demi Ultra (DU), Kerr, Orange, CA] were used. Specimen preparation, polymerization characterization, and beam profile quantification were performed as described in detail and illustrated

in previous work with a few modifications [30]. In this study, specimens were cured at 2- or 8-mm distances from the top. The study design is illustrated in Fig. 1.

Polymerization pattern characterization

Briefly, each light guide tip was centered over a Managing Accurate Resin Curing System-Resin Calibrator (MARC-RC) top sensor (Bluelight Analytics Inc., Halifax, Canada). The radiant exposure was maintained (10–11 J/cm²) by adjusting the curing time at each distance, using the manufacturer recommendation for a dual-photoinitiator RBC (Tetric EvoCeram bleaching shade XL, Ivoclar Vivadent, Amherst, NY, Lot# T25427). Square composite specimens (5 × 5 × 2 mm) were prepared using a Delrin mold made to standardize the specimen position. Six specimens were prepared for each LCU at each distance: three for the top and bottom characterization and three for depth characterization. Specimens were stored dry at 37 °C for 24 h [15, 25]. Depth characterization specimens were sectioned using a hard tissue microtome (Series 1000 Deluxe, Scientific Fabrications, Littleton, CO) with a 0.2-mm wafer blade (Buehler, Lake Bluff, IL, USA) at standardized locations. All specimens were finished and polished (Struers, Ballerup, Denmark), rinsed, and ultrasonically cleaned. KH mapping was performed on the top and bottom surfaces and on each slice harvested at standardized locations using an automated hardness stage (Clemex ST-2000 automatic stage, Norwood, MA) mounted on the hardness tester (Instron, Wilson-Tukon model 2100B, Norwood, MA), with a 50-g load and 10-s dwell time [27].

The next day, DC mapping was performed using micro-Raman spectroscopy (FORAM, CRAIC Technologies, San Dimas, CA) at standardized locations, five scans for each measurement point. Spectra of uncured composites ($n = 3$) were recorded. DC was calculated by comparing the relative change of the vinyl C=C band peak height at 1640 cm⁻¹ to an aromatic C=C reference band peak height at 1610 cm⁻¹. The DC calculation was performed using the following equation [31]:

$$DC\% = \left(1 - \frac{\text{cured (peak height at 1640/peak height at 1610)}}{\text{uncured (peak height at 1640/peak height at 1610)}} \right) \times 100$$

CLD mapping was performed using an ethanol-softening method with repeated microhardness measurements. Each specimen was placed in 1 ml of absolute ethanol (Sigma-Aldrich, St. Louis, MO, Lot# SHBF5121V) for 24 h and blot dried. KH mapping was then performed. The %KH reduction was calculated for each localized value before and after soaking the specimens in ethanol and used as a CLD surrogate throughout this manuscript.

3D and 2D renderings

DC, KH, and %KH reduction renderings were generated using ParaView 5.0 (Ayachit, Utkarsh, The ParaView Guide: A Parallel Visualization Application, Kitware, 2015, ISBN 978-1930934306). 3D renderings were generated after averaging the measurements of each point. 2D top renderings aided visualization of the association between the beam profile pattern and DC, KH, and %KH reduction.

Irradiance beam profile quantification

Briefly, beam profile images were generated using a CCD camera-based beam profiler system (BGP-USB-SP620 with a FL-50 CCTV lens, Ophir-Spiricon, North Logan, UT) combined with power values obtained with an optical spectrometer (FLAME-S-VIS-NIR, Ocean Optics, Dunedin, FL). The camera position was standardized and calibrated. Shortpass and longpass optical filters (Edmund Optics, Barrington, NJ), both with a cutoff wavelength of 425 nm, were used to collect violet and blue light, respectively, at 2- and 8-mm distances, for each LCU. Images were processed using BeamGage Professional software (5.11, Ophir-Spiricon, North Logan, UT). Radiant power from each LCU was collected using a 6-in. integrating sphere (Labsphere, North Sutton, NH) connected to a calibrated (HL-3plus-INT-CAL, Ocean Optics, Dunedin, FL) Ocean Optics optical spectrometer. Custom adapters that matched the dimensions of the active portion of each guide tip were placed over the integrating sphere opening at 2 and 8-mm distances. Radiant power measurements were collected for each LCU from the shortpass (380–425 nm) and longpass (425–700 nm) wavelength ranges ($n = 3$), and the average power value was applied to the corresponding image for each LCU to generate calibrated 2D irradiance distribution images. For each LCU, the respective values for the area of the active portion of the guide tip combined with its average power were used to calculate the spectral irradiance of the LCU and determine the percentage contributions from the violet and blue chips.

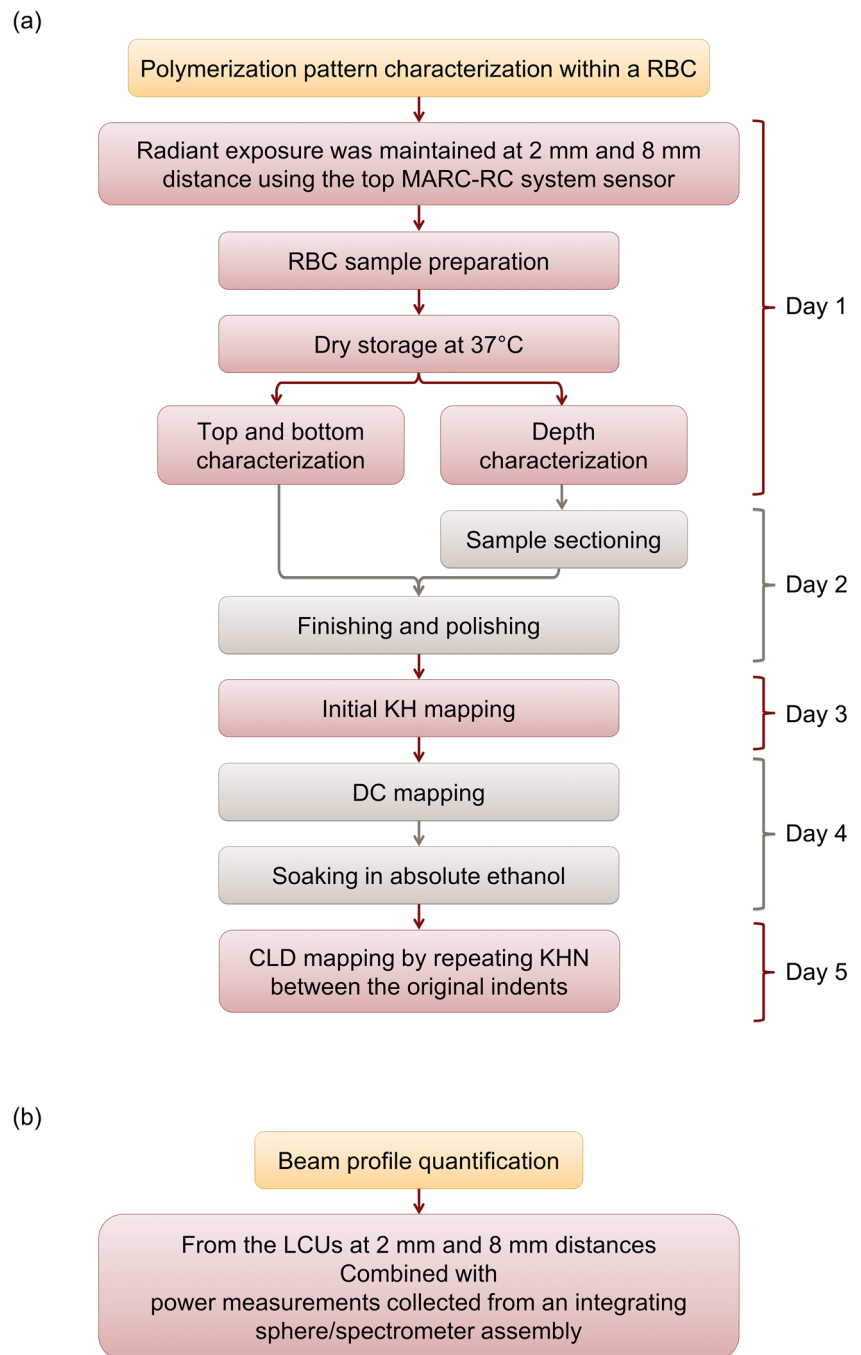
Correlations

The numerical localized average irradiance values of each square in the grid were correlated with the corresponding localized DC, KH, and %KH reduction values at each distance.

Statistical analyses

The effects of different LCUs and at 2- or 8-mm curing distances on an RBC DC, KH, and %KH reduction, were analyzed using ANOVA. Each LCU-distance combination was allowed to have

Fig. 1 Study design. **a** Polymerization pattern characterization within the RBC specimens. **b** Beam profile quantification



a different variance. Repeated measures ANOVA was used to explore the significant differences among points at each depth. The correlations among the measurements were based on the distance between them. Linear mixed models were used to calculate the correlations across multiple locations on each specimen while accounting for within-specimen correlations. Pearson correlation coefficients were used for the associations of the localized irradiance values with the corresponding localized DC, KH, and %KH reduction values on the top surfaces. Normality assumptions were met for all analyses. The homogeneous variance assumption was met for the ANOVAs ($\alpha = 0.05$).

Results

Polymerization pattern characterization

Polymerization patterns were not uniform within the specimens regardless of the curing distance (Figs. 2 and 3). The DC did not follow a specific pattern where the QTH and MLED units yielded higher localized DC values than the SLED units, regardless of distance. Using the QTH and MLED units, a gradual decrease in KH appeared from the top to the bottom, and a gradual increase in %KH reduction

values indicated a higher CLD on the top. However, using the SLED units showed a relatively uniform localized KH and %KH reduction distribution. Localized KH and %KH reduction values were higher at the 8-mm than the 2-mm distance. The localized bottom/top KH ratios were greater than 80% with few exceptions at the 2-mm distance when using O, V, SM, and D, and when using BS, V, and O at the

8-mm distance (Online Resource 1). The number of significant comparisons varied for each property, each LCU, and differed between 2 and 8-mm distances with no specific pattern (Tables 1, 2, and 3) ($p < 0.05$). Several significant interactions were observed between the LCUs and each measurement at specific depths (Online Resources 2, 3, and 4).

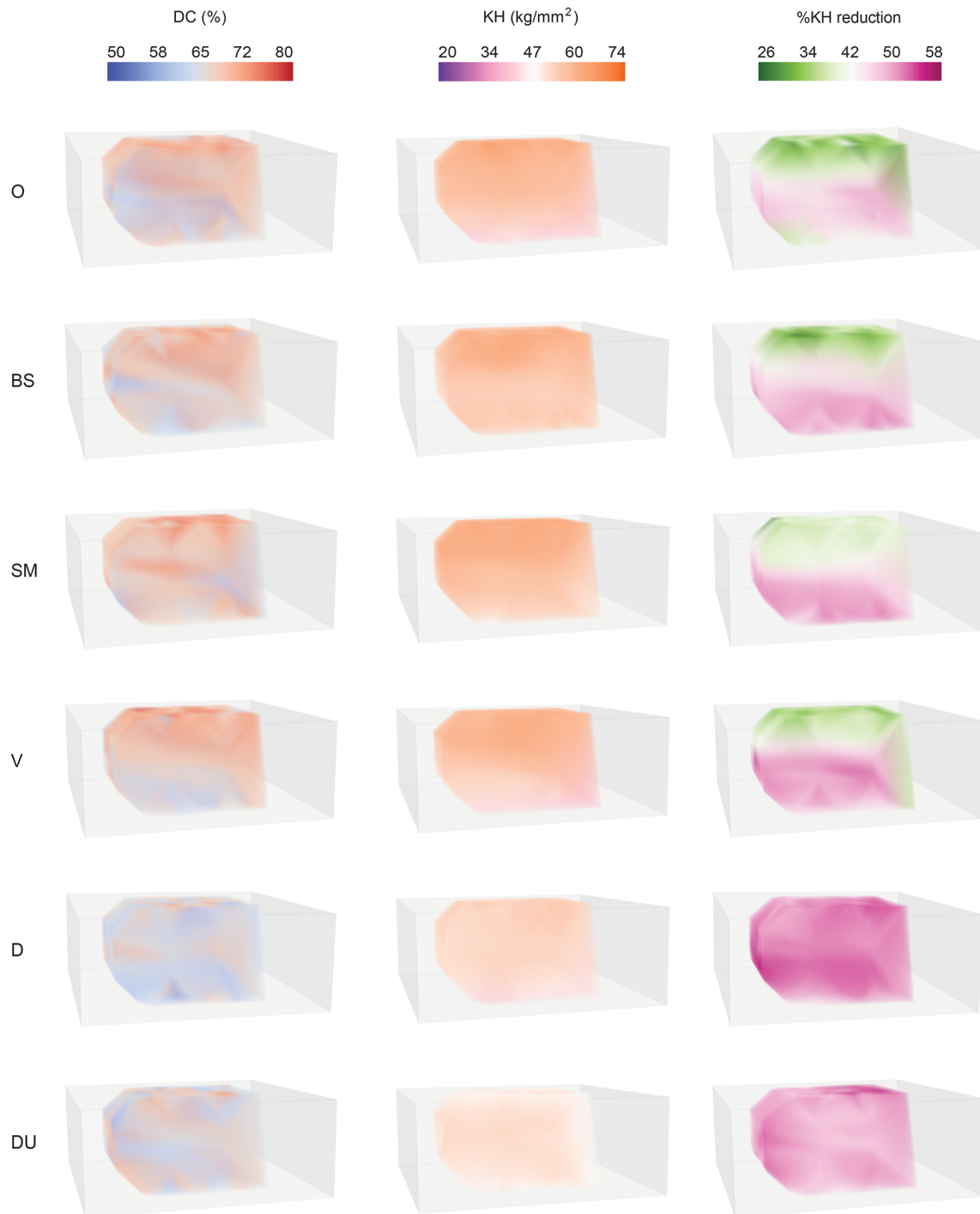


Fig. 2 3D renderings of the DC (%), KH (kg/mm²), and %KH reduction values within RBC specimens light cured using the LCUs explored at 2-mm curing distance

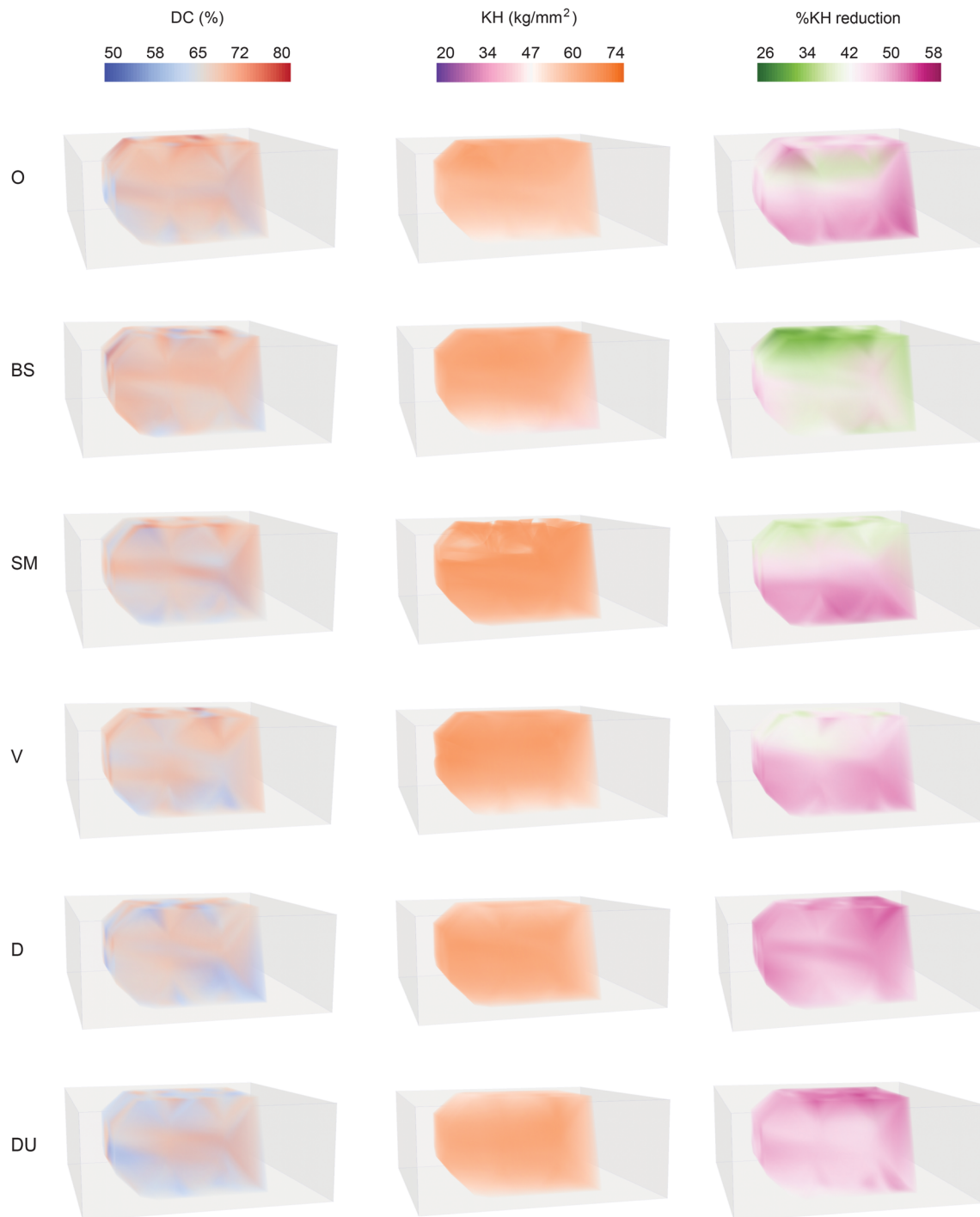


Fig. 3 3D renderings of the DC (%), KH (kg/mm^2), and %KH reduction values within RBC specimens light cured using the LCUs explored at 8-mm curing distance

LCU irradiance beam profile characterization

The characteristics for each LED unit varied (Table 4). The QTH had a broad spectral emission and included blue and violet ranges. The MLED units exhibited peaks in the blue and violet regions. The SLED lights had one peak in the blue region. The percent of irradiance from the QTH and MLED units was similar in the longer

wavelengths and greater than the shorter wavelengths (Fig. 4). The 2D irradiance beam profile images using the longpass filter quantified at each distance were coupled with the corresponding 2D renderings of the top surface measurements (Figs. 5 and 6). No unit provided a perfectly uniform irradiance distribution. Each LED unit had “hot-spots” and “cold-spots” that corresponded to the blue and violet LED chips,

Table 1 Number of localized significant comparisons (*) among the DC (%) measurement points of the RBC specimens across each depth and curing distance using the LCUs explored

Depth (mm)	*No. of comparisons	Distance (mm)	O	BS	SM	V	D	DU
0.0	1224	2	76	104	23	104	18	85
		8	84	136	60	53	78	26
0.5	104	2		18	0	6	0	11
		8	2	11	0	1	9	0
0.7	104	2	3	0	0	1	0	8
		8		0	0	0		0
0.9	104	2	6	30	2	14	12	5
		8	0	24	9	3	4	8
1.1	104	2	5	0	0	0	0	1
		8	3	7	12	0	15	15
1.3	104	2	4	0	2	4	7	21
		8		2		8	2	21
1.5	104	2	12	0	11	0	0	9
		8	5	2	0	9	12	0
2.0	104	2	94	10	52	65	112	64
		8	51	40	78	122	62	38
Total	3288	2	212	162	101	194	149	213
		8	150	224	159	205	194	108

*1224 comparisons among measurement points on the top or bottom surfaces/LCU/distance. 104 comparisons among measurement points across each depth/LCU/distance. 3288 sum comparisons from all measurements across each depth/LCU/distance. Fewer significant differences indicated that a more consistent DC was observed across the specimen for a LCU at any given depth. Missing entries in the table were due to lack of convergence for the model. The LCU that resulted in the least number of DC significant comparisons to the most number of significant comparisons was in the following order: at 2-mm curing distance: SM < D < BS < V < O < DU ($p < 0.05$); at 8-mm curing distance: DU < O < SM < D < V < BS ($p < 0.05$). Abbreviations: Optilux 401, O; Bluephase Style, BS; SmartLight Max, SM; Valo Cordless, V; Demi, D; Demi Ultra, DU

respectively. The beam profiles at 8 mm exhibited lower and relatively more uniform irradiance values over a wider area than 2 mm. At 2 mm, the average localized irradiance values ranged between 235 and 1600 mW/cm²; at 8 mm, ranged between 180 and 1005 mW/cm². The DC, KH, and %KH reduction patterns did not reflect the LCU irradiance patterns, regardless of distance. Non-uniform DC, KH, and %KH reduction distribution was exhibited across the top surfaces, which was more evident for the DC.

Correlation of localized DC with KH and %KH reduction

The correlation between the localized DC values and KH or %KH reduction values varied at each depth and curing distance for each LCU (Table 5). The localized correlation between DC and KH was moderate to weak at most depths regardless of the curing distance. A strong positive correlation was detected at 0.9-mm and 1.1-mm depths using BS at 2-mm distance, at 1.5-mm depth using DU at 2-mm distance, at 0.7-mm depth using O at 8-mm distance, at 2.0-mm depth using BS at 8-mm distance, and on the top using SM at 8-mm distance. The correlations between the

localized DC and %KH reduction values were mostly moderate regardless of the curing distance. A strong positive correlation was seen at 2 mm using BS and DU at 1.3-mm depth and at 8-mm curing distance using BS at 2.0-mm depth as was shown for SM on the top.

Correlations of the localized irradiance with top surface DC, KH, and %KH reduction

A weak correlation was exhibited between the localized irradiance values and the corresponding top surface DC, KH, and %KH reduction. A few significant correlations were detected; DC values were significantly correlated with irradiance values at 2 mm using V with a positive association using the longpass filter and a negative correlation using the shortpass filter. KH values were significantly associated with the irradiance values at 2 mm using V with a negative association using the longpass filter. At 8-mm distance, a negative association was seen using the longpass filter with BS and a positive correlation using the shortpass filter. The %KH reduction measurements showed a significantly positive association with the BS irradiance values at 8 mm using the longpass filter. All $p < 0.05$.

Table 2 Number of localized significant comparisons (*) among the KH (kg/mm^2) measurement points of the RBC specimens across each depth and curing distance using the LCUs explored

Depth (mm)	*No. of comparisons	Distance (mm)	O	BS	SM	V	D	DU
0.0	1224	2	72	24	8	16	80	33
		8	31	141	68	58	11	79
0.5	104	2	0	18	2	1	11	0
		8	0	1	6	2	0	0
0.7	104	2	4	21	1	9	3	7
		8	2	10	2	0	2	2
0.9	104	2	3	0	1	12	7	0
		8	0	4	0	1	16	3
1.1	104	2	0		4	7	8	3
		8	14	13	11	1	10	0
1.3	104	2	6	2	3	23	1	6
		8	0		1	0	13	0
1.5	104	2	0	0	1	8	3	4
		8	0	9	8	3	0	1
2.0	104	2	70	20	33	149	105	110
		8	13	294	11	37	97	34
Bottom/top ratio	990	2	42	25	8	30	30	65
		8	86	152	22	33	19	35
Total	3288	2	155	85	54	233	221	167
		8	60	481	115	105	149	120

*1224 comparisons among measurement points on the top or bottom surfaces/LCU/distance. 104 comparisons among measurement points across each depth/LCU/distance. 990 comparisons among bottom/top KH ratio measurement points/LCU/distance. 3288 sum comparisons from all measurements across each depth/LCU/distance. Fewer significant differences indicated that a more consistent KH was observed across the specimen for a LCU at any given depth. Missing entries in the table were due to lack of convergence for the model. The LCU that resulted in the least number of KH significant comparisons to the most number of significant comparisons was in the following order: at 2-mm curing distance: $\text{SM} < \text{BS} < \text{O} < \text{DU} < \text{D} < \text{V}$ ($p < 0.05$); at 8-mm curing distance: $\text{O} < \text{V} < \text{SM} < \text{DU} < \text{D} < \text{BS}$ ($p < 0.05$). The LCU that resulted in the least number of bottom/top KH ratio significant comparisons to the most number of significant comparisons was in the following order: at 2-mm curing distance: $\text{SM} < \text{BS} < \text{V} = \text{D} < \text{O} < \text{DU}$ ($p < 0.05$); at 8-mm curing distance: $\text{D} < \text{SM} < \text{V} < \text{DU} < \text{O} < \text{BS}$ ($p < 0.05$). Abbreviations: Optilux 401, O; Bluephase Style, BS; SmartLight Max, SM; Valo Cordless, V; Demi, D; Demi Ultra, DU

Discussion

Polymerization pattern characterization

With respect to DC, KH, and %KH reduction, non-uniform localized polymerization discrepancies were detected regardless of the LCU or curing distance with the non-uniformity being more evident in the DC values (Figs. 2 and 3). The location and number of significant differences among points at each depth differed regardless of the LCU or curing distance (Tables 1, 2, and 3). The types of RBC, specimen thickness, radiant exposure, and LCU position, were all standardized, in this study, in order to limit the confounding variables. Furthermore, the tested RBC contained CQ and TPO with less CQ concentration, compared to other shades of the same RBC. Therefore, a better assessment of the influence of a non-uniform beam on the corresponding polymerization pattern was expected [32]. Ultimately, the relationship between

the observed non-uniform polymerization patterns and the measurements collected from the specimens can be partially explained by the variations in the beam irradiance profiles, heat generated by the LCUs, the polymerization, filler particles, photoinitiator type, and light transmission through the specimens [3].

A portion of the heat generated during light curing is from the exothermic polymerization reaction [3, 33]. Temperature elevation can increase the rate of polymerization and cause the glass transition temperature of the resin to be reached at an earlier stage [3, 18]. In addition, mobility of the polymer chains decreases as polymerization proceeds and the viscosity of the resin matrix increases, leading to the entrapment of free radicals along with unreacted double bonds and pendant groups [3, 34]. Also, filler particle size, type, and distribution can impact the monomer mobility because they can restrict the diffusion of free radicals [3, 35]. The literature reports that 50–75% DC values are typically achieved when using a light-

Table 3 Number of localized significant comparisons (*) among the %KH reduction measurement points of the RBC specimens at each depth and curing distance using the LCUs explored

Depth (mm)	*No. of comparisons	Distance (mm)	O	BS	SM	V	D	DU
0.0	1224	2	100	50	48	10	55	65
		8	8	107	29	45	130	32
0.5	104	2	0	9	4	6	3	10
		8	1	4	5	12	8	0
0.7	104	2	0		0	7	8	4
		8	1	6		12	15	0
0.9	104	2	10	4	2		0	10
		8	3	10	3	1	25	1
1.1	104	2	7	3	4	14	11	1
		8	14		10	0	6	
1.3	104	2	3	4	0	13	21	12
		8		1	5	0	33	4
1.5	104	2	12	0	1	1	4	3
		8	2	7	0	0	0	
2.0	104	2	159	38	22	76	158	42
		8	39	93	74	16	65	80
Total	3288	2	303	108	82	128	264	150
		8	70	235	126	86	282	117

*1224 comparisons among measurement points on the top or bottom surfaces/LCU/distance. 104 comparisons among measurement points across each depth/LCU/distance. 3288 sum comparisons from all measurements across each surface and depth/LCU/distance. Fewer significant differences indicate that a more consistent %KH reduction was observed across the specimen for a LCU at any given depth. Missing entries in the table were due to lack of convergence for the model. The LCU that resulted in the least number of %KH reduction significant comparisons to the most number of significant comparisons was in the following order: at 2-mm curing distance: SM < BS < V < DU < D < O ($p < 0.05$), and at 8-mm curing distance: O < V < SM < DU < BS < D ($p < 0.05$). Abbreviations: Optilux 401, O; Bluephase Style, BS; SmartLight Max, SM; Valo Cordless, V; Demi, D; Demi Ultra, DU

activated conventional RBC [36]. Our results showed that localized mean DC values were greater than 50%, indicating that the total amount of light energy deposited on the specimens was sufficient for the expected conversion. A few random individual points had DC values that were less than 50%,

which were not evident after averaging the values of each localized point. The low values may be due to the localized entrapment of free radicals that could cause insufficient polymerization at specific locations [3]. It was reported that resins containing a TPO/CQ photoinitiator system tend to entrap

Table 4 Characterization of the LCUs explored. Effective light-emitting diameter (mm), number and type of the LED chips, spectral distribution peaks at the long and short spectral range (nm), and irradiance (mW/cm^2) for the LCUs explored using the integrating sphere/spectrometer assembly

LCU	Effective light-emitting diameter (mm)	Number of LED chips	Long wavelength spectrum (nm)		Short wavelength spectrum (nm)		Irradiance (mW/cm^2)			
			Blue	Violet	Range	Peak	Range	Peak	Blue range	Violet range
QTH	O	10.8	–	–	380–525	492	380–525	–	465	117
Multiple emission peak LED (MLED)	BS	9	2	1	426–525	454	381–426	408	760	146
	SM	*Area = 49 mm ²	1	1	417–510	446	380–417	398	1128	417
	V	9.7	2	1	420–525	447	380–420	394	539	135
			1 longer blue			458				
Single emission peak LED (SLED)	D	7.4	1	–	411–512	454	–	–	800	–
	DU	8	3	–	429–532	467	–	–	878	–

The long and short wavelength spectrum was collected at 2 mm away from the integrating sphere opening using the longpass and shortpass filters, respectively. The irradiance values were calculated from the average power (mW) measurements collected at 2 mm away from the integrating sphere opening using the effective light-emitting area of the individual LCU. Abbreviations: Optilux 401, O; Bluephase Style, BS; SmartLight Max, SM; Valo Cordless, V; Demi, D; Demi Ultra, DU

*Area value provided by the manufacturer

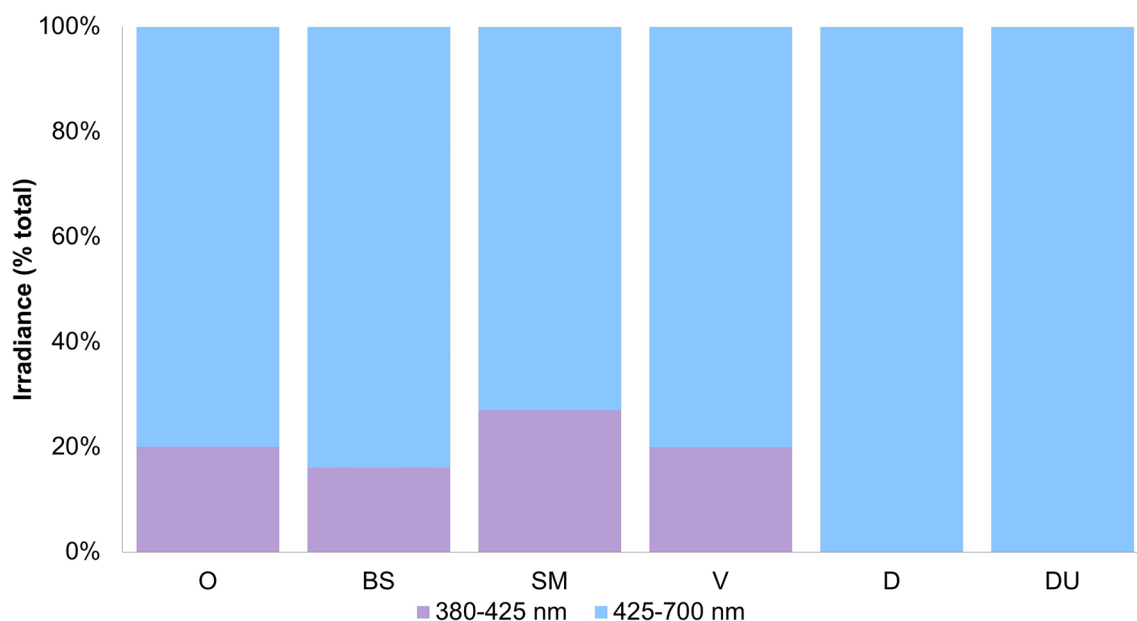


Fig. 4 Percentage (%) of total irradiance from the blue (425–700 nm) and violet (380–425 nm) spectral regions of the LCUs explored at 2-mm curing distance from the integrating sphere opening

more free radicals within the resin matrix [12]. A limitation of this study is that specimen polishing and handling prior to testing may have impacted DC values.

On the top surfaces, satisfactory polymerization was achieved regardless of the LCU used or the curing distance. Because of limited interference on the top [37], sufficient amounts of photoinitiator activation and free radical production take place [17, 19]. The amount of light striking the surface decreases as it travels through the resin and is absorbed by photoinitiators and pigments [3]. Filler particle size and geometry can impact light scatter and refraction at resin-filler interfaces, impacting polymerization at the deeper parts of the specimens [3, 35]. In addition, the Mylar strip placed on the top, absorbed 3.5–6.4% of the irradiance measured from the LCUs. This absorbance was similar in another study [26].

The photoinitiator system may partially explain the differences in uniformity of the KH and %KH reduction measurements in specimens cured by the QTH and MLED units compared to the SLED lights. TPO has a high molar absorptivity in the shorter wavelength region (380–420 nm) and tends to generate free radicals and a polymer network at a faster kinetic rate compared to CQ [35, 38, 39]. Therefore, TPO may have been prematurely spent via bimolecular termination before the polymer network was fully established. Also, the short wavelengths associated with the violet LED chips that peak at 394–408 nm, which are needed to activate TPO, may have scattered in the specimens, not effectively reaching the bottom compared to the longer wavelengths, which is associated with the blue LED chips that peak at 446–448 nm (Table 4) [3, 35, 38, 39]. This may have led to TPO entrapment within the resin matrix in the deeper portions of the specimens [10, 35].

Therefore, when using the SLED units, the relatively uniform polymerization observed may be because TPO was not effectively activated throughout the specimens. Our findings suggest that effective TPO activation decreases gradually up to approximately 1-mm depth (the middle), when using the QTH or MLED compared to the SLED units, regardless of the curing distance (Figs. 2 and 3). Interestingly, curing with the SLED units did not compromise polymerization with respect to DC and KH values, nor did it for the QTH or MLED on the bottom surfaces. This suggests that CQ concentration within the selected RBC was enough for satisfactory polymerization activation, when using the SLED lights. Also, the findings suggested that specimens received enough irradiance from the blue LED chips, which effectively activated CQ (Fig. 4). The findings were in partial agreement with the literature [40]. Our findings may translate to RBCs with similar composition, shade, and translucency and may differ to some extent when using different RBCs. Further investigation is needed to explore polymerization uniformity using RBCs with different photoinitiator systems.

Regarding the curing distance: higher localized KH and CLD values were measured at 8 mm compared to 2 mm regardless of the LCU. In this study, the radiant exposure was controlled, which may have allowed sufficient time for the photoinitiators to generate a suitable number of free radical growth centers for satisfactory polymerization [18, 26]. In addition, this may have resulted in a localized temperature increase in the specimen resin matrix, accelerating the reaction, but negatively impacting CLD. Therefore, the non-significant differences among the points at each depth with respect to the DC, KH, and %KH reduction values may be because the radiant exposure was kept constant.

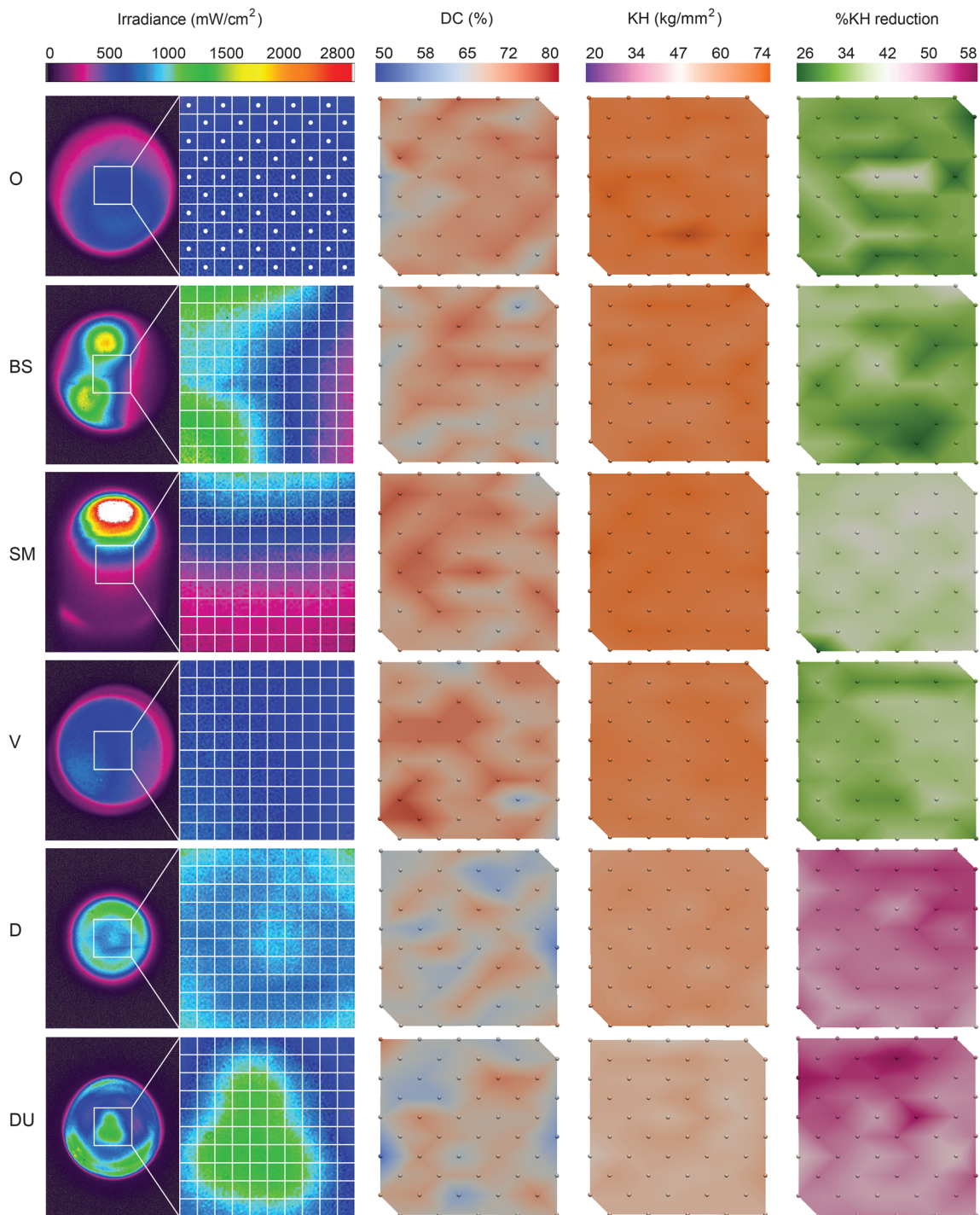


Fig. 5 2D images of the localized irradiance beam profiles from the LCUs explored, measured through a 425-nm longpass filter coupled with the corresponding 2D localized DC, KH, and %KH reduction values on the top specimen surfaces at 2-mm distance from the target surface. The white squares at the center of each image correspond to the

3 × 3-mm area on the specimens where the DC and KH measurements were collected. Each 3 × 3-mm area was divided into a 10 × 10 grid. Each square in the grid, using a localized average irradiance value calculated from 1156 pixels, was correlated with the corresponding localized DC, KH, and %KH reduction values

Assessment of the bottom/top hardness ratio is an indicator of curing effectiveness of RBCs, and, although somewhat arbitrary, 80% has been suggested as the minimally acceptable ratio [41]. The previously discussed localized differences in heat, light transmission, and entrapment of

free radicals could explain the localized bottom/top KH ratios that were less than 80% (illustrated in Online resource 1). When curing the RBC specimens using the SLED, the essential absence of points (except one) that were less than 80% may indicate that the various regions of the specimens

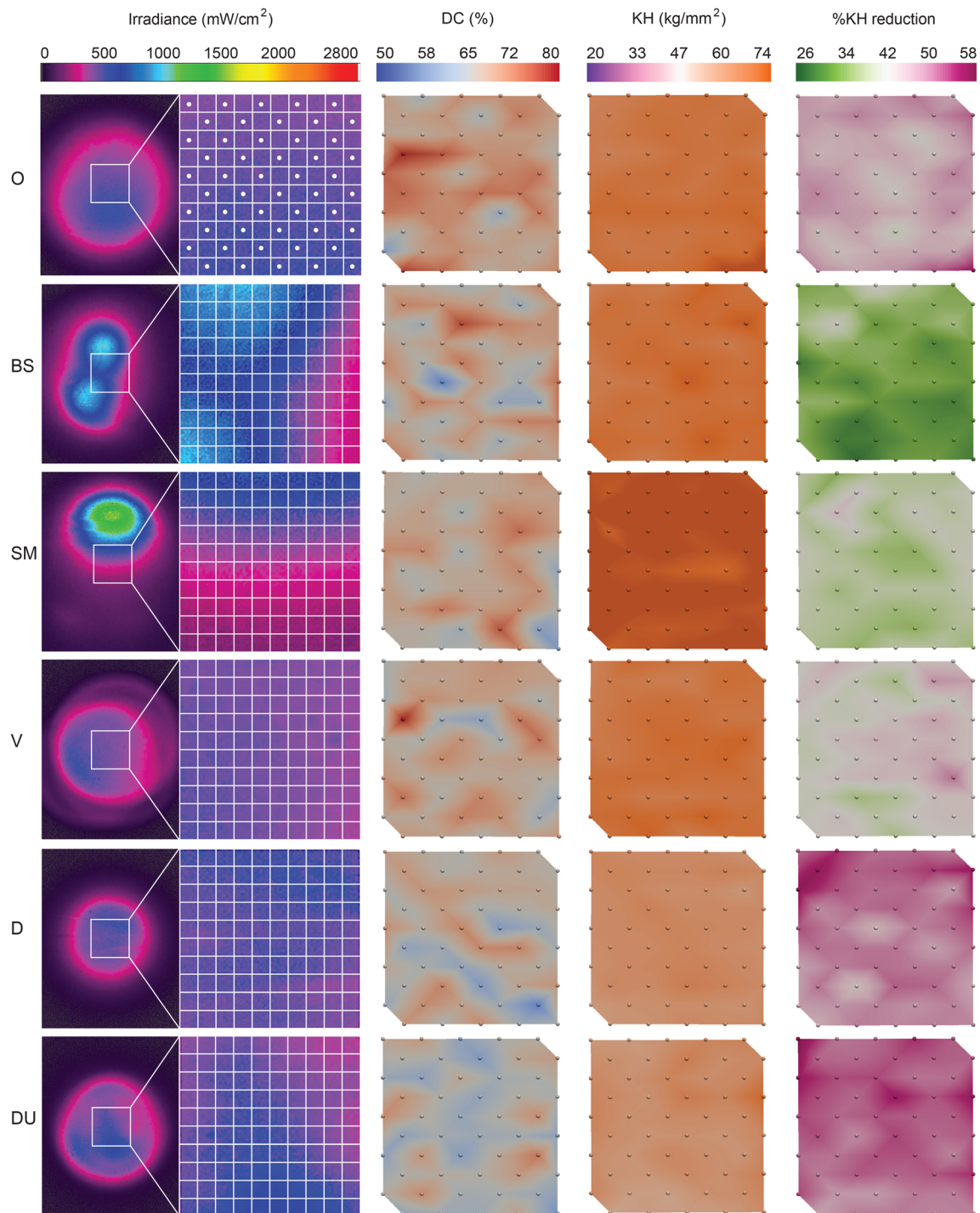


Fig. 6 2D images of the localized irradiance beam profiles from the LCUs explored, measured through a 425-nm longpass filter coupled with the corresponding 2D localized DC, KH, and %KH reduction values on the top specimen surfaces at 8-mm distance from the target surface. The white squares at the center of each image correspond to the

received sufficient irradiance leading to satisfactory polymerization throughout the specimens. However, a bottom/top KH ratio that is greater than 80% did not necessarily indicate that the specimen polymerization was uniform across its top and bottom. This was evident when a LCU

3×3 -mm area on the specimens where the DC and KH measurements were collected. Each 3×3 -mm area was divided into a 10×10 grid. Each square in the grid, using a localized average irradiance value calculated from 1156 pixels, was correlated with the corresponding localized DC, KH, and %KH reduction values

resulted in localized bottom/top KH ratios greater than 80%, but exhibited significant differences among those localized points (Table 2).

The findings confirm that a mapping approach to evaluate polymerization effectiveness provides more details than by

Table 5 Correlations for the localized DC values with the corresponding KH, and %KH reduction values using the different LCUs at 2 and 8-mm curing distances

LCU	Depth (mm)	Distance			
		2 mm		8 mm	
		KH	%KH reduction	KH	%KH reduction
O	0.0	-0.25	0.13	-0.79	-0.60
	0.5			-0.25	0.37
	0.7	-0.60	-0.51	0.84	
	0.9	0.63	0.11	-0.69	0.45
	1.1	0.39	0.35	-0.03	0.18
	1.3	0.27	0.54	-0.19	-0.51
	1.5	-0.70	-0.89	0.74	-0.73
BS	2.0	0.66	0.23	-0.01	-0.32
	0.0			-0.70	-0.61
	0.5	0.19	-0.49	-0.35	-0.60
	0.7	-0.43		-0.34	0.43
	0.9	0.86	0.25	-0.23	-0.38
	1.1	0.75	0.61	0.18	0.09
	1.3	0.51	0.86	-0.37	-0.44
SM	1.5	-0.39		-0.27	-0.35
	2.0	0.25	0.09	0.88	0.83
	0.0	-0.62	-0.29	0.81	0.80
	0.5	-0.11	-0.45	0.51	0.56
	0.7	0.31	0.22	-0.55	-0.32
	0.9	0.08	0.06	0.24	-0.19
	1.1	-0.62	0.15	-0.29	0.68
V	1.3	0.06	0.41	-0.30	-0.42
	1.5	-0.66	-0.71	-0.13	-0.05
	2.0	-0.38	-0.21	0.17	0.47
	0.0	-0.02		-0.42	-0.28
	0.5	-0.68	-0.41	-0.24	0.11
	0.7	-0.60	-0.39	-0.02	-0.16
	0.9	0.71	0.61	0.05	0.17
D	1.1	-0.80	-0.41	-0.23	-0.42
	1.3	0.44	-0.72	0.64	0.02
	1.5	-0.55	0.12	-0.41	-0.47
	2.0	0.41	0.43	0.08	-0.03
	0.0	-0.15	-0.59	0.66	0.48
	0.5	-0.70	-0.42	0.30	0.39
	0.7	-0.47	-0.38		
DU	0.9	-0.18	0.11	-0.76	-0.55
	1.1	0.00	0.24	-0.58	-0.57
	1.3	-0.12	0.61	0.47	0.41
	1.5	0.50	-0.29	0.26	-0.30
	2.0	-0.45	0.59	-0.17	0.09
	0.0			-0.30	0.13
	0.5	0.29	0.41	0.21	0.26
	0.7	0.44	-0.20	-0.19	-0.12
	0.9	-0.30	0.33		0.20
	1.1		0.41	0.64	0.63
	1.3	0.50	0.79	-0.08	0.18
	1.5	0.75	0.34	0.45	0.57
	2.0	0.10	0.63	0.59	0.21

Correlation coefficients are missing when the correlation could not be estimated by the linear model. Abbreviations: Optilux 401, O; Bluephase Style, BS; SmartLight Max, SM; Valo Cordless, V; Demi, D; Demi Ultra, DU

using average values across each depth, as performed in most studies. This is evident in the additional data given in Online Resource 5, which show several interesting findings

when the values of all the points were averaged across each depth compared to the localized points (Figs. 2 and 3). The Online Resource 5 showed significant differences among curing units with respect to their effect on DC, KH, and %KH reduction values. For each LCU, significant differences were detected between 2 and 8-mm curing distances across each depth with respect to KH values, but few significant differences were found with respect to DC and %KH reduction values. The average bottom/top KH ratio across the surfaces showed only O at 2 mm that exhibited a ratio of less than 80% compared to the other units and curing distances, unlike when using the localized points.

LCU irradiance beam profile characterization

Each LCU varied in its full spectral range and peak wavelength (Table 4). In addition, the relative irradiance contribution from the longer and shorter wavelength ranges was similar among the QTH and MLED lights (Fig. 4). The findings were similar to another study that demonstrated relative variation in LED chip radiant power from multiple lights [23]. Also, the irradiance distribution of the beam profile varied for each LCU. Interestingly, the polymerization patterns, with respect to the DC, KH, and %KH reduction maps, did not reflect the LCU irradiance patterns (Figs. 5 and 6). The QTH (O) exhibited a somewhat more uniform beam irradiance profile because its light source is a tungsten filament that emits wavelengths over a wide spectral range [19, 20, 22]. The variation in the “hot-spots” in the MLED and SLED irradiance beam profile images can be explained by the variation in the number, location, and the type of the LED chips used [18, 20, 21, 24, 25, 42]. When using a longpass filter, the “hot-spot” regions on the irradiance distribution images for the BS and SM (Fig. 5) corresponded to the blue LED chips with spectral emission peaks approximately between 446 and 454 nm, which overlaps the absorption spectrum for CQ [18, 21, 24, 25]. The low-irradiance regions on the images corresponded to the locations of the violet LED chips with spectral emission peaks ranging from 398 to 408 nm [21, 25]. The decreased irradiance distribution in the images at 8-mm compared to 2-mm curing distance was consistent with the divergence of the emitted light over distance, resulting in less radiant power striking the same area [21, 28, 29, 42]. For each LCU, regardless of the curing distance, the overall average irradiance values were greater than 400 mW/cm², which is internationally considered to be the minimum irradiance for sufficient polymerization [43]. However, some squares of the irradiance grids on the irradiance beam profiles of the LCUs were lower than 400 mW/cm². For example, at 2-mm curing distance, SM was measured to have an average irradiance value of 1532 mW/cm². However, one localized square on the irradiance grid had an irradiance value of 235 mW/cm², which decreased to 180 mW/cm² at 8-mm distance. Nevertheless,

polymerization was acceptable at that specific point with the DC = 59.6% and the KH = 66 kg/mm². Previous work showed that the mean irradiance values across the surface significantly decreased at the bottom of 2-mm-thick specimens compared to the values on the top [30]. Also, the literature has similarly shown that irradiance profiles passing through specimens decreased from the top to the bottom [44, 45]. Thus, we can expect that the localized irradiance values will also decrease as light from the curing units passes through the specimens to the bottom. Characterizing a limited LCU area is a weakness in this study; however, polymerization discrepancies within the RBC were shown. The outcomes suggest that the LCUs do not result in uniform polymerization regardless of the curing distance, which further supports the complexity of polymerization kinetics. Therefore, the first and second working hypotheses can be generally accepted. The outcomes suggest that uniform polymerization does not occur which may contribute to restoration fracture. Further investigation is needed to assess the influence of non-uniform polymerization on a restoration's mechanical properties and fracture.

Correlations of localized DC with KH and %KH reduction values

The correlations of the localized DC values with KH and %KH reduction values were generally moderate to weak (Table 5). Nevertheless, the correlations at each depth varied with LCU and curing distance. This was explained throughout this manuscript. For this reason, the third working hypothesis was rejected. On the other hand, additional data provided in Online Resource 6 showed that the correlations of the average DC values with the average KH and %KH reduction values across each depth were generally strong, and they also varied at each depth for each LCU. These outcomes suggest that using the average DC, KH, and %KH reduction values across each depth, as performed in most studies, could provide artificially high correlations, as has been mentioned before.

Correlations of localized irradiance beam area with DC, KH, and %KH reduction

The findings show that the localized polymerization values on the top specimen surfaces were not compromised, although the irradiance beam profiles coming from the LCUs were weakly correlated to the respective localized DC, KH, and %KH reduction values. Therefore, the fourth working hypothesis was rejected. This further supports that it is possible that the irradiance beam profile coming from a curing unit may not greatly influence the polymerization patterns of an RBC. Note that the correlations of the irradiance beam profiles with the DC, KH, and %KH reduction values, at the remaining depths, could not be accomplished because the beam profile software that was used exports only 2D data.

Conclusions

Based on the findings of the limited irradiance areas measured from six LCUs and a dual-photoinitiator RBC assessed at two clinically relevant curing distances, the following were concluded: (1) Investigating multiple material properties through a mapping approach within a RBC cured at clinically relevant distances provided a more detailed characterization of polymerization occurring within the RBC. (2) There was no LCU that created similar polymerization patterns at all localized points assessed within the specimens with respect to DC, KH, and %KH reduction regardless of curing distance. (3) The non-uniform irradiance beam profiles did not seem to have a major influence on the localized polymerization discrepancies within the specimens with respect to DC, KH, and %KH reduction at both curing distances. (4) The SLED units used in this study did not compromise polymerization of the dual-photoinitiator RBC. (5) Effective TPO activation decreases gradually up to approximately 1-mm depth using the QTH or MLED compared to the SLED units, regardless of the curing distance. (6) Correlations of the DC values with the corresponding KH and %KH reduction at the localized points within the specimens were moderate to weak and varied for each LCU, depth, and curing distance. (7) The irradiance beam profiles from the LCUs were weakly correlated with DC, KH, and %KH reduction for the RBC at both curing distances.

Acknowledgments The work is part of the PhD dissertation for Dr. A. O. Al-Zain. The scholarship support from King Abdulaziz University, Jeddah, Saudi Arabia, and the technical assistance received from UITS/PTI Advanced Visualization Lab at Indiana University are acknowledged.

Compliance with ethical standards

Conflict of interest The authors declare that they have no conflict of interest.

Ethical approval This article does not contain any studies with human participants or animals performed by any of the authors.

Informed consent For this type of study, formal consent is not required.

Publisher's note Springer Nature remains neutral with regard to jurisdictional claims in published maps and institutional affiliations.

References

1. Demarco FF, Collares K, Coelho-de-Souza FH, Correa MB, Cenci MS, Moraes RR, Opdam NJ (2015) Anterior composite restorations: a systematic review on long-term survival and reasons for failure. *Dent Mater* 31:1214–1224. <https://doi.org/10.1016/j.dental.2015.07.005>

2. Alvanforoush N, Palamara J, Wong RH, Burrow MF (2017) Comparison between published clinical success of direct resin composite restorations in vital posterior teeth in 1995–2005 and 2006–2016 periods. *Aust Dent J* 62:132–145. <https://doi.org/10.1111/adj.12487>
3. Leprince JG, Palin WM, Hadis MA, Devaux J, Leloup G (2013) Progress in dimethacrylate-based dental composite technology and curing efficiency. *Dent Mater* 29:139–156. <https://doi.org/10.1016/j.dental.2012.11.005>
4. Ferracane JL (2013) Resin-based composite performance: are there some things we can't predict? *Dent Mater* 29:51–58. <https://doi.org/10.1016/j.dental.2012.06.013>
5. Cramer NB, Stansbury JW, Bowman CN (2011) Recent advances and developments in composite dental restorative materials. *J Dent Res* 90:402–416. <https://doi.org/10.1177/0022034510381263>
6. Ferracane JL, Mitchem JC, Condon JR, Todd R (1997) Wear and marginal breakdown of composites with various degrees of cure. *J Dent Res* 76:1508–1516
7. Soh MS, Yap AU (2004) Influence of curing modes on crosslink density in polymer structures. *J Dent* 32:321–326. <https://doi.org/10.1016/j.jdent.2004.01.012>
8. Li J, Li H, Fok AS, Watts DC (2009) Multiple correlations of material parameters of light-cured dental composites. *Dent Mater* 25:829–836. <https://doi.org/10.1016/j.dental.2009.03.011>
9. Durner J, Obermaier J, Draenert M, Ilie N (2012) Correlation of the degree of conversion with the amount of elutable substances in nano-hybrid dental composites. *Dent Mater* 28:1146–1153. <https://doi.org/10.1016/j.dental.2012.08.006>
10. Santini A, Miletic V, Swift MD, Bradley M (2012) Degree of conversion and microhardness of TPO-containing resin-based composites cured by polywave and monowave LED units. *J Dent* 40:577–584. <https://doi.org/10.1016/j.jdent.2012.03.007>
11. Leprince JG, Leveque P, Nysten B, Gallez B, Devaux J, Leloup G (2012) New insight into the “depth of cure” of dimethacrylate-based dental composites. *Dent Mater* 28:512–520. <https://doi.org/10.1016/j.dental.2011.12.004>
12. Selig D, Haenel T, Hausnerova B, Moeginger B, Labrie D, Sullivan B, Price RB (2015) Examining exposure reciprocity in a resin based composite using high irradiance levels and real-time degree of conversion values. *Dent Mater* 31:583–593. <https://doi.org/10.1016/j.dental.2015.02.010>
13. Rencz A, Hickel R, Ilie N (2012) Curing efficiency of modern LED units. *Clin Oral Investig* 16:173–179. <https://doi.org/10.1007/s00784-010-0498-3>
14. Ilie N, Stark K (2014) Curing behaviour of high-viscosity bulk-fill composites. *J Dent* 42:977–985. <https://doi.org/10.1016/j.jdent.2014.05.012>
15. Schneider LF, Moraes RR, Cavalcante LM, Sinhoreti MA, Correr-Sobrinho L, Consani S (2008) Cross-link density evaluation through softening tests: effect of ethanol concentration. *Dent Mater* 24:199–203. <https://doi.org/10.1016/j.dental.2007.03.010>
16. Alshali RZ, Salim NA, Satterthwaite JD, Silikas N (2015) Post-irradiation hardness development, chemical softening, and thermal stability of bulk-fill and conventional resin-composites. *J Dent* 43:209–218. <https://doi.org/10.1016/j.jdent.2014.12.004>
17. Yap AU, Soh MS, Han TT, Siow KS (2004) Influence of curing lights and modes on cross-link density of dental composites. *Oper Dent* 29:410–415
18. Price RB, Ferracane JL, Shortall AC (2015) Light-curing units: a review of what we need to know. *J Dent Res* 94:1179–1186. <https://doi.org/10.1177/0022034515594786>
19. Rueggeberg FA (2011) State-of-the-art: dental photocuring—a review. *Dent Mater* 27:39–52. <https://doi.org/10.1016/j.dental.2010.10.021>
20. Rueggeberg FA, Giannini M, Arrais CAG, Price RBT (2017) Light curing in dentistry and clinical implications: a literature review. *Braz Oral Res* 31:e61. <https://doi.org/10.1590/1807-3107BOR-2017.vol31.0061>
21. Megremis SJ, Ong V, Lukic H, Shepelak H (2014) An ada laboratory evaluation of light-emitting diode curing units. *J Am Dent Assoc* 145:1164–1166. <https://doi.org/10.14219/jada.2014.97>
22. Jandt KD, Mills RW (2013) A brief history of LED photopolymerization. *Dent Mater* 29:605–617. <https://doi.org/10.1016/j.dental.2013.02.003>
23. Harlow JE, Sullivan B, Shortall AC, Labrie D, Price RB (2016) Characterizing the output settings of dental curing lights. *J Dent* 44:20–26. <https://doi.org/10.1016/j.jdent.2015.10.019>
24. Michaud PL, Price RB, Labrie D, Rueggeberg FA, Sullivan B (2014) Localised irradiance distribution found in dental light curing units. *J Dent* 42:129–139. <https://doi.org/10.1016/j.jdent.2013.11.014>
25. Price RB, Labrie D, Rueggeberg FA, Sullivan B, Kostylev I, Fahey J (2014) Correlation between the beam profile from a curing light and the microhardness of four resins. *Dent Mater* 30:1345–1357. <https://doi.org/10.1016/j.dental.2014.10.001>
26. Haenel T, Hausnerova B, Steinhaus J, Price RB, Sullivan B, Moeginger B (2015) Effect of the irradiance distribution from light curing units on the local micro-hardness of the surface of dental resins. *Dent Mater* 31:93–104. <https://doi.org/10.1016/j.dental.2014.11.003>
27. Price RB, Fahey J, Felix CM (2010) Knoop microhardness mapping used to compare the efficacy of LED, QTH and PAC curing lights. *Oper Dent* 35:58–68. <https://doi.org/10.2341/09-055-L>
28. Platt JA, Price RB (2014) Light curing explored in Halifax. *Oper Dent* 39:561–563. <https://doi.org/10.2341/1559-2863-39.6.561>
29. Price RB, Labrie D, Whalen JM, Felix CM (2011) Effect of distance on irradiance and beam homogeneity from 4 light-emitting diode curing units. *J Can Dent Assoc* 77:b9
30. Al-Zain AO, Eckert GJ, Lukic H, Megremis SJ, Platt JA (2018) Degree of conversion and cross-link density within a resin-matrix composite. *J Biomed Mater Res B Appl Biomater* 106:1496–1504. <https://doi.org/10.1002/jbm.b.33960>
31. Albino LG, Rodrigues JA, Kawano Y, Cassoni A (2011) Knoop microhardness and FT-Raman evaluation of composite resins: influence of opacity and photoactivation source. *Braz Oral Res* 25:267–273
32. Palin WM, Senyilmaz DP, Marquis PM, Shortall AC (2008) Cure width potential for MOD resin composite molar restorations. *Dent Mater* 24:1083–1094. <https://doi.org/10.1016/j.dental.2008.01.001>
33. Mousavinasab SM, Meyers I (2011) Comparison of depth of cure, hardness and heat generation of LED and high intensity QTH light sources. *Eur J Dent* 5:299–304
34. Beun S, Bailly C, Dabin A, Vreven J, Devaux J, Leloup G (2009) Rheological properties of experimental Bis-GMA/TEGDMA flowable resin composites with various macrofiller/microfiller ratio. *Dent Mater* 25:198–205. <https://doi.org/10.1016/j.dental.2008.06.001>
35. Leprince JG, Hadis M, Shortall AC, Ferracane JL, Devaux J, Leloup G, Palin WM (2011) Photoinitiator type and applicability of exposure reciprocity law in filled and unfilled photoactive resins. *Dent Mater* 27:157–164. <https://doi.org/10.1016/j.dental.2010.09.011>
36. Vasudeva G (2009) Monomer systems for dental composites and their future: a review. *J Calif Dent Assoc* 37:389–398
37. Watts DC, Cash AJ (1994) Analysis of optical transmission by 400–500 nm visible light into aesthetic dental biomaterials. *J Dent* 22:112–117
38. Ikemura K, Endo T (2010) A review of the development of radical photopolymerization initiators used for designing light-curing dental adhesives and resin composites. *Dent Mater J* 29:481–501
39. Vaidyanathan TK, Vaidyanathan J, Lizymol PP, Ariya S, Krishnan KV (2017) Study of visible light activated polymerization in

- BisGMA-TEGDMA monomers with type 1 and type 2 photoinitiators using Raman spectroscopy. *Dent Mater* 33:1–11. <https://doi.org/10.1016/j.dental.2016.09.002>
40. Sampaio CS, Atria PJ, Rueggeberg FA, Yamaguchi S, Giannini M, Coelho PG, Hirata R, Puppini-Rontani RM (2017) Effect of blue and violet light on polymerization shrinkage vectors of a CQ/TPO-containing composite. *Dent Mater* 33:796–804. <https://doi.org/10.1016/j.dental.2017.04.010>
 41. Moore BK, Platt JA, Borges G, Chu TM, Katsilieri I (2008) Depth of cure of dental resin composites: ISO 4049 depth and microhardness of types of materials and shades. *Oper Dent* 33:408–412. <https://doi.org/10.2341/07-104>
 42. Corciolani G, Vichi A, Davidson CL, Ferrari M (2008) The influence of tip geometry and distance on light-curing efficacy. *Oper Dent* 33:325–331. <https://doi.org/10.2341/07-94>
 43. ISO (2007) 10650-2:2007 dentistry-powered polymerization activators: part 2: light-emitting diode (LED) lamps. Geneva, Switzerland: International Standards Organization.:7
 44. Harlow JE, Rueggeberg FA, Labrie D, Sullivan B, Price RB (2016) Transmission of violet and blue light through conventional (layered) and bulk cured resin-based composites. *J Dent* 53:44–50. <https://doi.org/10.1016/j.jdent.2016.06.007>
 45. Shimokawa C, Sullivan B, Turbino ML, Soares CJ, Price RB (2017) Influence of emission spectrum and irradiance on light curing of resin-based composites. *Oper Dent* 42:537–547. <https://doi.org/10.2341/16-349-L>